Simulations of Tracking Gold Nanorods with Two-Photon Scanning Microscopy in 3D

THESIS

submitted in partial fulfillment of the
requirements for the degree of

MASTER OF SCIENCE
in
PHYSICS

Author :	J Culkin
Student ID :	S1574272
Supervisors :	John van Noort
	Sara Carozza
2^{nd} corrector :	Thomas Schmidt

Leiden, The Netherlands, March 22, 2016

Simulations of Tracking Gold Nanorods with Two-Photon Scanning Microscopy in 3D

J Culkin

Huygens-Kamerlingh Onnes Laboratory, Leiden University
P.O. Box 9500, 2300 RA Leiden, The Netherlands

March 22, 2016

Abstract

Complex cellular processes can be characterised using single particle tracking techniques (SPT). 'Labels' such as metal nanoparticles are introduced into cells and tracked to reveal molecular trajectories. Many current techniques are based on fluorescence microscopy, and have nanometre-resolution. To accurately probe cellular processes, a technique must also have long-term 3D in-vivo observing capability with a minimal toxic effect. Gold nanorods (GNRs) in two-photon microscopy is a promising technique. GNRs are non-toxic, easily functionalisable, and exhibit a bright two-photon fluorescence. However, the theoretical positional accuracy for this technique is not yet known. Furthermore, the detailed trajectory data present statistical challenges. We have addressed these issues here numerically, using simulated image data. We found the accuracy to be between 5.2 nm and 8.9 nm for stationary GNRS, dependent on the separation between slices. We also found that diffusive movement of a nanorod lowers the accuracy, at worst case to 31.8 nm. We have also investigated optimising the extraction of behaviour properties from MSD plots, and have used Welsh's test to detect transitions. GNRs in two-photon microscopy has been shown to be a very accurate technique, and its trajectory data can yield accurate behavioural information. The fit of the PSF may be improved, but the techniques already compares well against others.

Contents

Chapter 1

Introduction

Complex cellular processes can be characterised by tracking individual molecular dynamics using single particle tracking techniques. Many current techniques are based on fluorescence microscopy, and are able to bypass diffraction-limited positional accuracy, in some cases under 10 nm, and often in 3D [1]. They involve tracking 'label' particles that attach to target molecules and emit optical signals upon excitation. Widely used and studied labels include fluorophores (fluorescent proteins/dyes), quantum dots and metal nanoparticles. The positions of labels smaller than the diffraction limit ($\lesssim 250$ nm) are 'super-resolved' by fitting the diffraction-limited spots in images with theoretical models, and extracting their centres. In order to precisely study long-term cellular processes the requirement are: high positional accuracy, high temporal accuracy, label stability (how long it lasts before bleaching/blinking), and label inertness (the lack of a steric or toxic effect on its environment). A common limitation is the inability to track long-term due to photobleaching and blinking. Another common limitation is time-resolution, restricting observation to slow moving particles. Tracking in 3D can also present challenges and limitations, for example in the technique reported by Levi et al, which involved tracking fluorescent polystyrene beads with two-photon microscopy [2]. They reported a positional accuracy of 20 nm, but were limited to particle velocity below $3\,\mathrm{m\,\mu s^{-1}}$ in the z-direction.

Two-photon scanning microscopy with gold nanorods (GNRs) as labels is a promising technique that enables in vivo long-term 3D nanometre resolution tracking. Van der Broek et al [3] found that isolated GNRs can be localized with a resolution of 4 nm in the xy-plane and 8 nm in the z-direction. Comparable accuracy of 20 nm has been achieved with fluorophores [4], and 10 nm with quantum dots [5]. However, both these labels

are subject to photobleaching, which prevents trajectories lasting longer than a few minutes, whilst individual GNRs have been tracked in cells in 3D for over 30 minutes [3]. Quantum dots are also subject to blinking, and both fluorophores and quantum dots present toxicity and fuctionalisation challenges - whilst GNRs are easily functionalised and are non-toxic.

The advantages of this technique, however, do come with challenges. For example the accuracy and limitations of the 3D 'super-resolution' fitting technique are not fully understood. Additionally, we must make sense of multiple long trajectories in a single FOV in which particles may change behaviour. In this thesis, we work toward a better understanding of these challenges and limitations by studying simulations.

First, we address the positional accuracy. Whilst a theoretical estimate of the positional accuracy in the case of 2D super-resolution single-particle tracking is known [6], we are not aware of any for the 3D case. Our hypothesis is that the xy-plane positional accuracy will be higher in the 3D case, due to the larger number of photons collected (see 1.3 for the full argument). In simulations we found that indeed the accuracy is higher in the 3D case.

Next, we addressed trajectory analysis. MSD analysis of GNR trajectories have revealed four types of motion: immobile, ballistic (e.g. active transport by motor proteins), confined diffusion (e.g within vesicles), and free diffusion (e.g in the cytoplasm) [3]. To differentiate and quantify these behaviours, trajectories are typically analysed using mean-square-displacement (MSD) plots: the shape of the plots are distinctively different for each behaviour, and desired properties can be extracted by fitting the plots: the diffusion coefficient D, the velocity v and the positional accuracy σ_p. The accuracy with which the MSD plots can be used to calculate these properties depends upon several factors including the number of positional measurements, the positional accuracy and the number of points in the MSD plots itself, as outlined in [7] and [8]. This thesis works to establish how the accuracy is affected by controllable factors in measurement and analysis.

Finally, we addressed the effect of diffusive movement on positional accuracy. In the scanning microscope, 3D images (stacks) are created by sequentially acquiring 2D images (slices) over a range in the z-direction. It is not known to what degree the positional accuracy is affected by the movement of the particle between the acquisition of the slices in a stack. In simulations we found that diffusive movement lowered the positional accuracy considerably, shown in section 2.5.

1.1 Two-photon fluorescence scanning microscopy

In our two-photon scanning microscope, a near-infrared femtosecond-pulsed laser is split by a diffractive optical element (DOE) into a 10x10 array of beams. The array scans across the entire sample plane (x,y), exciting the fluorophores. The subsequent luminescence from the sample is captured by a CCD camera positioned back along the optical track, and a 3D image is built by scanning multiple slices in the z-direction. A detailed description of the set-up has been given in [3]. In one-photon fluorescence microscopy, the photons used to excite the label particles interact with and damage the biological samples, and produce an out-of focus back-scattering that strongly impacts on the signal/noise ratio [9]. Two-photon techniques mitigate these problems by using lower energy near-infrared photons. As they interact only weakly with the biological matter, they produce only weak back-scattering, improving the signal/noise ratio, and damaging the sample less.

Two-photon fluorescence microscopy typically involves using label particles with an excitation energy approximately double the energy of the laser photons. Only when a high flux is provided, there is a (low) possibility that the label particles in the FOV will absorb two photons simultaneously. The excitation of small metal particles such as GNRs is different however: in both one-photon and two-photon cases, the incoming energy of the photon must be close to the energy of the plasmon resonance, as described in the next section. The advantage of two-photon fluorescence, is that the probability of the (simultaneous) absorption, depends not linearly, but quadratically on the excitation intensity [9]. The intensity of the emitted signal corresponds to the amount of absorption, so this too depends quadratically on the excitation intensity. Thus, by focusing a very short pulsed laser on the sample, the chance of simultaneous absorption can be maximised without using a high power that would damage the sample. The quadratic dependence on the intensity and tight focusing of the laser result in the luminescence being confined to the focal spot. This, together with the lower wavelength of light used, results in a much higher signal/noise ratio and decreased level of damage to the sample compared with single-photon microscopy.

1.2 Gold nanorods

Gold nanorods exhibit a strong plasmon-enhanced two-photon luminescence, can be easily functionalized, and have been shown to be nontoxic,

making them a good label for in vivo two-photon fluorescence microscopy [3]. Plasmons are quasiparticles: they are the quantum associated with collective oscillations of the free electron gas with respect to the fixed ion lattice in the metal. Due to their elongated shape, gold nanorods exhibit two surface-confined plasmons, in the longitudinal and latitudinal directions. The two-photon luminescence is due to the plasmon excitation and relaxation. It is strongly enhanced if the wavelength of the incident photons is such that they couple with the longitudinal surface plasmon. [10].

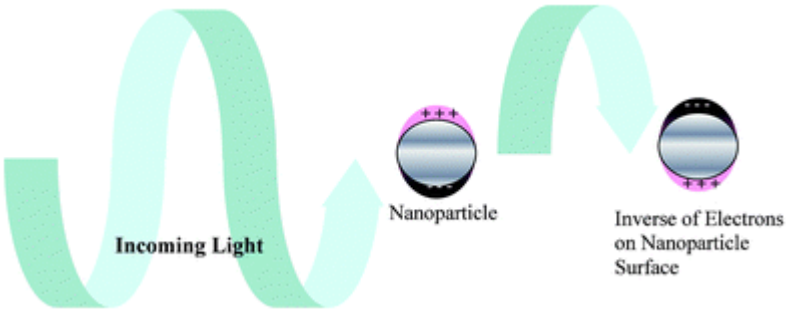

Figure 1.1: Surface Plasmon. *In this image the electron density in the particle is polarized to one surface and then the other: a surface plasmon is formed which oscillates in resonance with the incoming light. The incident photons on gold nanorods couple to the same plasmon, boosting the luminescence significantly. Image from Eustis and El-Sayed [11].*

Since the aspect ratio of the gold nanorods determines the wavelength of the surface plasmons, their size can be chosen so that the wavelength suits one's requirements. In our case, this means we are able to use near infra-red excitation photons - which are minimally absorbed by water and biological samples [10]. Using gold nano rods in the two-photon scanning microscope allows not only 3D positioning, but also a vast increase in signal strength compared with other labels, for example 58 times that of Rhodamine [12].

1.3 Positional accuracy

The positional accuracy of an imaging system is the minimal distance at which separate structural details can be distinguished. The theoretical best accuracy for any conventional optical microscope, also known as the diffraction limit, was first approximated by Abbe [13]. He approximated the minimal distance possible d to be about half of the wavelength λ of

the light used, but dependent also on the numerical aperture of the microscope, $N_A = n \sin\theta$, which is a measure of the range of angles θ it accepts, and the refractive index n of the medium through which the light travels.

$$d = \frac{\lambda}{2N_A} \tag{1.1}$$

As light passes through the specimen, it diffracts and spreads out radially. This, together with the interfering nature of waves results in a pattern in the focal plane due to a point source called the Airy disk: a central spot surrounded by concentric diffraction rings. The accuracy of a microscope then relies on distinguishing between separate Airy disks, which is limited by their size - which is precisely d given above. Typical microscopes with $N_A \sim 1$ and $\lambda \sim 500\,\text{nm}$ are then limited in accuracy to $\sigma_p \sim 250\,\text{nm}$. However there are now many 'super-resolution' techniques which are able to bypass the diffraction limit.

The position of an object smaller than the diffraction limit can be found in super-resolution imaging: the centre of the diffraction-limited spot it produces in the image is extracted by fitting its distribution with a known theoretical model [14]. In our set-up, the two-photon florescence spot of a single GNR is approximately Gaussian shaped [14]. We are therefore able to super-resolve its position by fitting a 3-dimensional Gaussian intensity profile to the spot observed in the fluorescence image:

$$I(x,y,z,t) = A_0 + A\exp\left[-\frac{(x(t)-x_c)^2}{2\sigma_x^2} - \frac{(y(t)-y_c)^2}{2\sigma_y^2} - \frac{(z(t)-z_c)^2}{2\sigma_z^2}\right] \tag{1.2}$$

An initial guess taken directly from the image is given for the parameters: the amplitude of the peak A, the offset (average background value) A_0, the width of the peak in each direction σ_x, σ_y, σ_z, and the centre x_c, y_c and z_c. The fit is performed by the method of least-squares fit.

Each photon collected gives a measure of the particle's position, with an error given by the width of the PSF of the microscope. With no other information, the best estimate of the position of the GNR would be simply the mean of these locations. The theoretical positional accuracy of this fitting method is not known. However, an estimate has been derived by Thompson et al. [6] for the similar case of fitting a 2D Gaussian, also by

the method of least squares:

$$\sigma_p = \sqrt{\frac{\sigma_{xy}^2}{N_p} + \frac{a^2}{12N_p} + \frac{8\pi\sigma_{xy}^4 b^2}{a^2 N_p^2}} \tag{1.3}$$

σ_{xy} is the standard deviation of the point spread function (PSF), N_p is the total amount of collected photons in each captured image, a is the pixel size and b is the standard deviation of the background noise (in photons). The first term in equation 1.3 corresponds to the inherent statistical error due to this averaging. The second term corresponds to pixelation: smaller pixels enable more precise locations to be given for where the photons hit the detector. The third term corresponds to background noise and depends on the signal-to-noise ratio. Our hypothesis is that the the positional accuracy in the xy-plane in 3D should be better than in the case of a single 2D image, as each additional slice in the 3D stack increases the total number of collected photons. If all the slices in a stack were projected into one image, that image could be fit as if it were 2D, and though blurred, it would offer an increase in the number of photons compared with a single 2D slice. This will be addressed in section 2.3.

The positional accuracy relies on the 3D Gaussian being a good approximation to the PSF. It has been shown that the dipole PSF is actually a better description for GNRs, however the Gaussian profile is robust, computationally inexpensive and has been shown to provide an accuracy better than 5 nm [14]. However, fitting a 3D Gaussian presents a novel problem: due to the finite time between slice acquisitions, the PSF will be deformed if the movement of the particle is comparable with the speed of the slice acquisition. This would cause the best fit of the Gaussian to return incorrect centre positions. The case of diffusive movement would be particularly troublesome, as the PSF may not be simply slanted as in the ballistic case, but totally deformed. As it is not known to what extent the positional accuracy would be affected, this is addressed in section 2.5.

1.4 Trajectory analysis

Tracked particles typically display one or a combination of the following behaviours: freely diffusive motion, ballistic motion, or confined diffusive motion. In cells, for example, these behaviours could correspond to, respectively, free Brownian movement in the cytoplasm; active transport of a motor protein or cellular organelle; or confinement within an organelle,

for example a vesicle. These different modes of mobility can be quantitatively distinguished by the mean square displacement (MSD) of the particle, as a function of time delay τ.

$$\mathrm{MSD}(\tau) \equiv \langle (x(t) - x(t+\tau))^2 \rangle \tag{1.4}$$

For a trajectory of total time length $T \geq \tau$, the MSD is the mean of the square displacement over all such periods of duration τ within the trajectory, When we calculate the MSD over a range of time delays and plot MSD(τ) against τ, the different modes of mobility result in distinctively different plots.

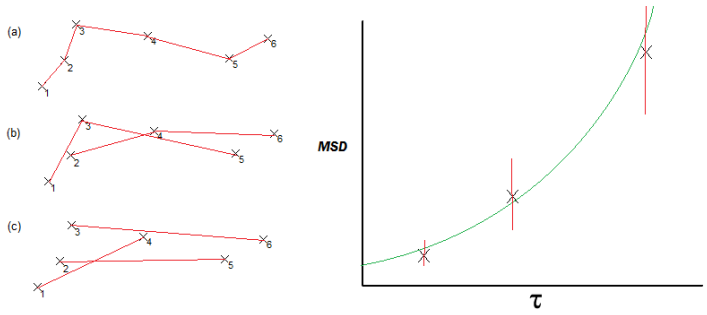

Figure 1.2: Illustration of mean-square-displacement calculation and plot. *Left: A trajectory of points separated each by* 1 s *on which the MSD is to be calculated for three values of* τ*, from* 1 s *to* 3 s*. MSD(τ) is the average of the square length of the distance between points separated in time by* τ*. Right: A plot with a line of best fit and error bars. The larger* τ*, the fewer values averaged and so the more uncertainty.*

A theoretical derivation of the MSD for a purely diffusing particle has been long known [15], in terms of the diffusion coefficient D, a measure of how fast a species of particle diffuses into a given environment. In purely free diffusion, a particle explores its environment as a 'random walk' - steps are taken of variable lengths in random directions, which results in the displacement from the origin to grow in proportion to the square-root of the number of steps, so the MSD grows linearly. When a particle is undergoing ballistic motion - that is, its velocity is constant - its displacement from a given location grows linearly with time, and so the MSD will grow quadratically. In measured trajectories, the positional accuracy of the measurement also affects the MSD plot by introducing an offset equal to its square. This can be understood by considering a plot of measurements of a fixed particle. Though the particle is fixed, the measurements of its location will form a Gaussian of width σ_p, indistinguishable from diffusive

motion confined within a small region of size σ_p. These three factors can be expressed in a single polynomial equation [7]:

$$MSD(\tau) = 2d\sigma_p^2 + 2dD\tau + v^2\tau^2 \tag{1.5}$$

The MSD is given in terms of the dimensions in the system d, the diffusion coefficient D, the ballistic velocity v, the positional accuracy of measurement σ_p, and the length of time delays τ over which it is calculated. By fitting this equation to an MSD plot for a given trajectory, we can acquire the value of these parameters of motion, and so quantitatively distinguish the the mode of mobility. If one of the parameters is already known, then that parameter can be fixed with the aim to improve the accuracy of the fit of the other parameters. The effect of fixing parameters is explored in section 2.4.2.

The number of points used in an MSD plot strongly affects the accuracy of the fit. Each point in an MSD plot is itself a statistical measure on a sample, so its accuracy is dependent on the size of that sample. Qian et al [7] have derived an estimated upper bound to the expected relative error in D (defined as $\delta_D = (D_{Detected} - D_{Actual})/D_{Detected}$), as a function of the total number of positional measurements N, and the number of points in the MSD plot n:

$$\delta_{D_{max}} = \pm\sqrt{\frac{2}{3}}\sqrt{\frac{n}{N-n}} \tag{1.6}$$

With typical values of $N = 150$ and $n = 15$ and an extracted value of $D = 0.5\,\mu m^2\,s^{-1}$, the formula predicts $\approx$ 27% relative error, and so our measurement is given as $D = 0.5 \pm 0.1\ \mu m^2\,s^{-1}$. Clearly, for a given value of N, this measure is minimised by taking the smallest value of n - suggesting that our MSD plots would give the most reliable estimates of D when using only 2 points. However, this estimate is purely statistical, and is based on the assumption of perfect positional accuracy. It may be a good estimate in cases of high positional accuracy, or with very large values of D, or a combination of both, but we must be sure first that we are in that region to make the assumption. We address this in section 2.4.1.

Michalet has extended the work of Qian et al, by taking into consideration the presence of positional accuracy in measurement, and has derived a theoretical expression for an optimal number of points to use in an MSD plot to improve the fit [8]. When τ increases, the stochasticity of the MSD dominates, preventing accurate calculation of the MSD and thus fitting -

on the other hand, the variation of the first few points on the MSD plot is dominated by the positional accuracy. Mitchalet defines the *reduced localisation error* x as the critical parameter to assess to determine the optimum number of MSD points to use:

$$x = \frac{\sigma_p^2}{D\Delta t} \tag{1.7}$$

It is given in terms of the positional accuracy σ_p, the diffusion coefficient D and Δt, the time between position measurements. He has assessed the relative error resulting in fitting the MSD curves over a range of values of x. For experimental conditions considered here, $\Delta t = 1$, $\sigma_p < 10\,\text{nm}$ and $0.01 \leq D \leq 1\ \mu\text{m}^2\,\text{s}^{-1}$, so $0.0001 \leq x \leq 0.1$. Mitchalet's theory then predicts that using $n = 2$ MSD points gives the most accurate extracted diffusion coefficient in all cases.

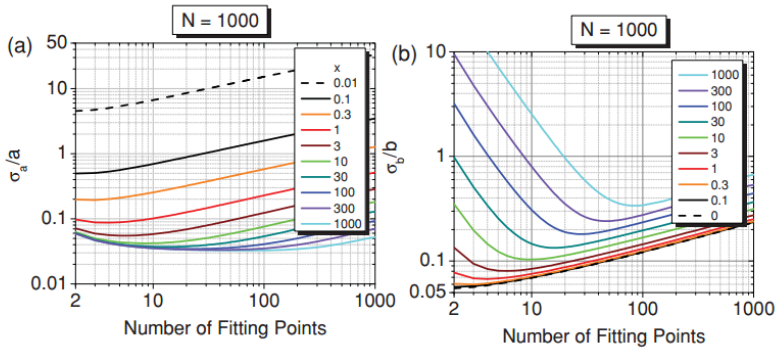

Figure 1.3: Relative error in fitting MSD plots. *Plots from Mitchalet's paper [8] showing the numerically determined relative error in fitting MSD plots of purely diffusive 2D trajectories, for a range of values of the reduced localisation error x. The parameters used by Mitchalet are $a = 4\sigma_p^2$ and $b = 4D$ (a) The relative error in fitting the intercept a, corresponding to the positional accuracy. (b) The relative error in fitting the slope b, corresponding to the diffusion coefficient. It is shown that the slope is far more sensitive, so choosing the optimal number of points is more important for it accurately extracting the diffusion coefficient*

When $x << 1$, for example corresponding to high positional accuracy and/or fast diffusive movement, then the best estimates come from using only the first two points of the MSD curve (excluding the (0,0) point). When $x >> 1$, for example with low positional accuracy and/or slow diffusive movement, the standard deviation of the first few MSD points are large, so higher numbers of MSD points must be used for reliable extracted

parameters [8]. In general, an optimal number of points $n_{optimal}$ can be found that balances the two effects at each extreme. Mitchalet found numerically an approximate fit for the optimal number of points, valid over trajectories of length 10 to 1000 steps [16]*:

$$n_{\text{optimal}} = 2 + 2.3x^{0.52} \tag{1.8}$$

As our experimental conditions and set-up may be different to those of Mitchalet et al., the predictions for n_{optimal} have been tested in section 2.3.

The accuracy of a point scales with the square root of the number of squared displacements that contribute to the point. This means that MSD points calculated at large τ should be weighted less. To do this, we would need to weight each point by the inverse of its variation. However, as there is not a theoretical expression for the variance, it should be estimated from data. Or the weighting could be approximated simply by $\sqrt{N}$, where N is the size of the sample over which the point is calculated. However, Mitchalet et al found that there is an optimum number of MSD points to use, in which case weighted and unweighted fits give similar accuracy [8].

Finally, in tracking particles, we are not only interested in the accuracy of estimating behavioural parameters - but also in how those parameters change in time, indicating changes in behaviour. For example, a particle freely diffusing in a cell, that attaches to a protein and is transported to a vesicle will display clear periods of differing behaviour. The behaviour change could also indicate a transient event, e.g. the particle picked up by the motor protein is immediately dropped again. In order to detect such behaviour changes we can plot the parameters we extract from the MSD plots calculated over rolling windows each of length N_w - the choice of which affects the accuracy of parameter measurement by determining both the maximum time period τ and N, the number of position measurements. We can then use statistical methods to quantitatively assess if and when behaviour changes have occurred. In section 2.4, we report on the success of using Welsh's test to do this.

*This is the revised version of the formula published in an erratum.

Chapter 2

Results

2.1 Simulating GNRs

3D stacked images characterising the 2-photon luminescence of single GNRs were captured using our microscope. Two samples were imaged: GNRs immobilized on glass slides, and GNRs injected into live HeLa cells. Figure 2.1a shows a typical example of a stacked image of the 2-photon luminescence intensity of a single GNR on a glass slide, and figure 2.2a shows a plot of a line segment of the intensity profile through the central slice.

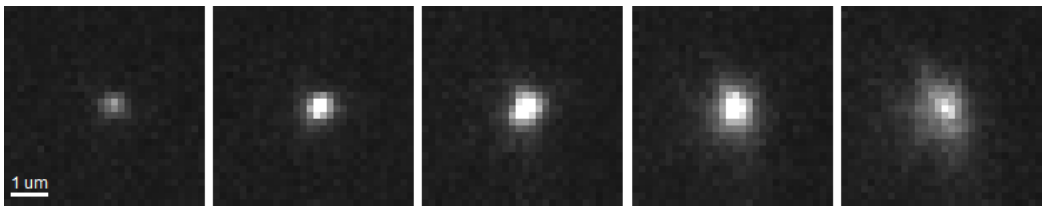

(a)

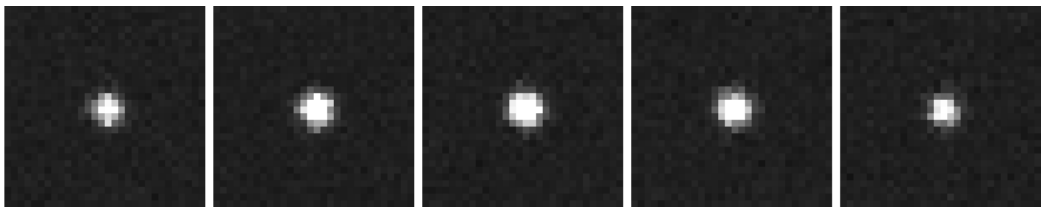

(b)

Figure 2.1: Real and simulated GNRs *Shown here are examples of* 5.25 µm *x* 5.25 µm *stacks with separation between slices of* 0.4 µm. ***(a)*** *shows a typical GNR immobilised on a glass slide.* ***(b)*** *shows a GNR simulated with average properties. The same contrast has been used in each case for direct comparison.*

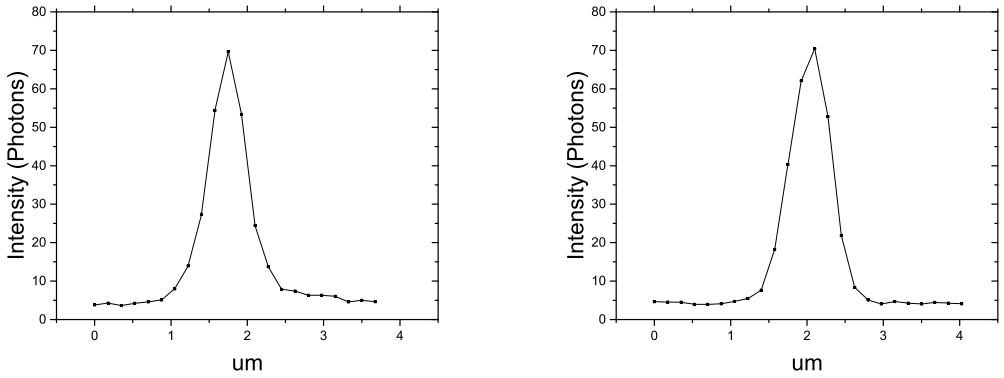

(a) **(b)**

Figure 2.2: Profiles of typical and simulated GNRs *Plots of line segments through the central slices of the 2-photon luminescence intensity images of GNRs shown in figure 2.1.* ***(a)*** *is from the real GNR, and* ***(b)*** *is from the simulated GNR.*

Real images was analysed using LabView to establish ranges and averages of the properties required for simulation. The point spread functions (PSF) were fitted with Gaussian distribution profiles:

$$I(x,y,z) = I_0 + A\exp\left[-\frac{(x-x_c)^2}{2\sigma_x^2} - \frac{(y-y_c)^2}{2\sigma_y^2} - \frac{(z-z_c)^2}{2\sigma_z^2}\right] \tag{2.1}$$

A is the peak amplitude, I_0 is the average background intensity; σ_x, σ_y and σ_z are the widths of the profile in each dimension; and the distribution is centred on x_c, y_c and z_c. The average background intensity I_0 is just an offset, and does not effect the accuracy of the fit. However, the noise on the background alters the signal-to-noise ratio and does affect the fit. We assumed the background noise to have a Gaussian distribution centred on I_0, with a width of b.

$$p(I_b) = \frac{1}{\sqrt{2\pi b^2}}\exp\left[-\frac{(I_b - I_0)^2}{2b^2}\right] \tag{2.2}$$

For each image, we removed the bright peaks and found the standard deviation b of the intensity values of the remaining pixels.

Histograms presenting the properties (PSF widths, number of photons and background widths) resulting from fitting a sample of 40 GNRs are shown in figure 2.3. The PSFs were of approximately equal width in the

x and y direction, and the combined average was 0.251 µm. The average Z width σ_z was larger at 0.679 µm. The mean number of total photons collected from a peak N_p was 3600 (note that this depends on the z-separation, which is here 0.4 µm), and the average background noise was 0.5 photons.

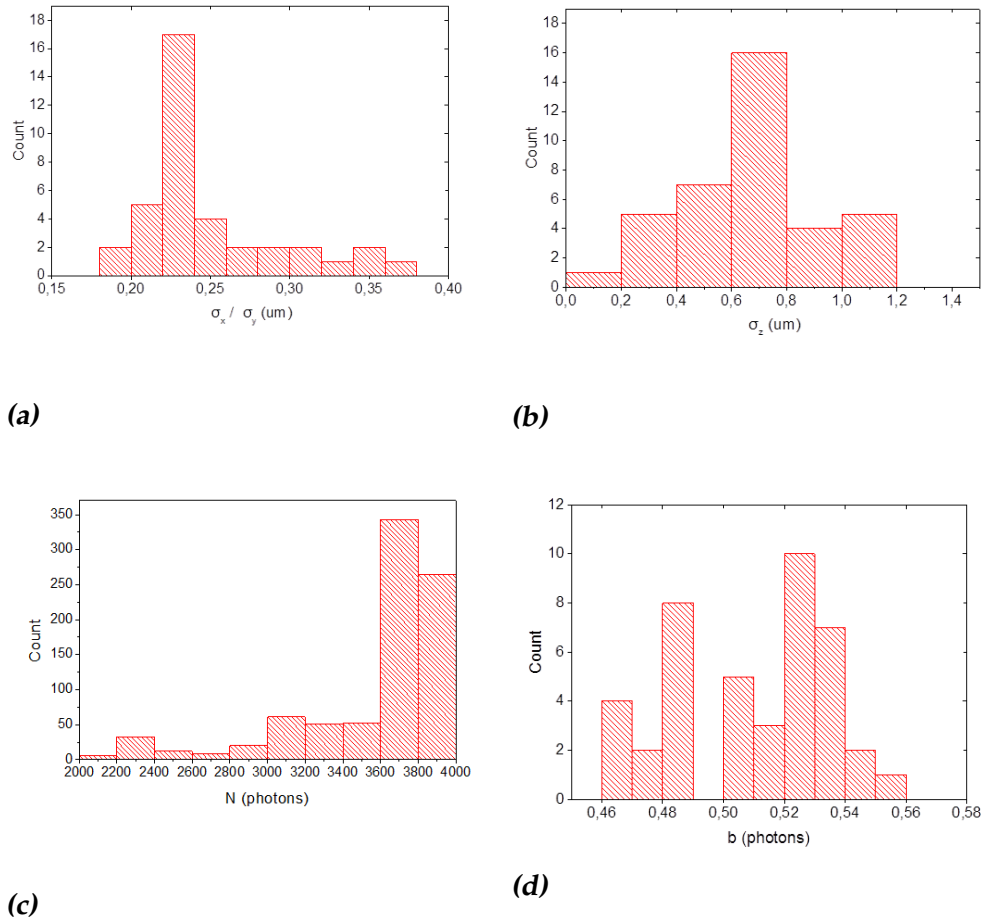

Figure 2.3: Properties of GNR point spread functions. *A sample of 40 GNRs from 10 videos (both in cell, and fixed on glass) were analysed to determine typical PSF properties.* ***(a)*** *shows the x-y width.* ***(b)*** *shows the z-width.* ***(c)*** *shows the total number of photons per GNR in a stack (this stack is made of 5 2D slices separated in the z-direction by* 0.4 µm. ***(d)*** *shows the background noise: b is the width of the Gaussian distribution fitted to the background.*

Simulations of 2-photon luminescence images of single GNRS were built in LabView in four steps, the last three of which are shown in figure 2.4

1. Position time-series $x(t), y(t), z(t)$ were created according to specified values of D and v. In the case of free diffusion, in each dimension and in each time step t the movement made was sampled from a Gaussian of standard deviation $2Dt$.

2. The number of photons collected by each pixel in the 3D field of view was set according to a 3D Gaussian as in equation 2.1. (See fig. 2.4a). I_0 was set to an arbitrary value, as it is only a offset and so does not impact the fitting process.

3. To account for photon shot-noise, the value of each pixel was then reset to $I(x,y,z,t) \rightarrow Poisson[I(x,y,z,t)]$, a value drawn at random from a Poisson distribution centred on $I(x,y,z,t)$. (See fig. 2.4b)

4. Finally a background noise of standard deviation b was added to the entire field of view. (See fig. 2.4c)

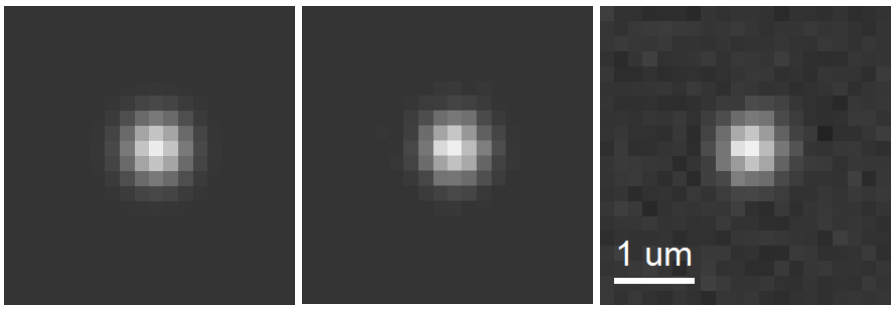

(a) ***(b)*** ***(c)***

Figure 2.4: GNR 2-photon intensity (2D) image simulated in three steps. (2.4a) *a Gaussian intensity distribution was first created with width $s = 0.250\,\mu m$, amplitude $A = 80$ photons, and a resultant total $N_{photons} = 1118$ (This is a single 2D slice).* ***(2.4b)*** *Shot noise was implemented.* ***(2.4c)*** *Lastly a background noise was added of a typical width $b = 0.5$ photons. The contrast is set here to make the background addition clear. See figure 2.1 for a side-by-side comparison of a real and simulated stack (note the contrast and scale is not the same as here).*

2.2 Image analysis

The simulated images were analysed with the same method as real images, by fitting a Gaussian profile to the intensity distribution due to the photons on the field of view (FOV). In each 3D stack of images, the brightest pixel was identified, and a 3-dimensional section (the "region of interest" ROI) around it was selected. This small section should contain a single GNR. The selection was then fitted with a Gaussian profile whose 3-dimensional centre determined the position of the GNR in the stack. If there was more than one GNR in the FOV, the algorithm then returns to the stack data and locates the next brightest spot - however the simulations here were restricted to the simplest case of just one GNR per FOV, in order to prevent incorrect assignment of a peak to a different trace. To then assess the positional accuracy of the measurements, the difference was calculated between the original co-ordinates used to generate the simulated GNR images and the co-ordinates determined by the fitting procedure. This was done for a large set of images, and the positional accuracy was taken as the standard deviation of the errors.

Numerical accuracy

First, we checked that the numerical accuracy was sufficiently high and could be neglected. We simulated 1000 3D stacks of images (each stack made of 10 2D slices) each containing a single randomly placed GNR, without background noise, nor shot noise (as in figure 2.4a). The co-ordinates set and calculated via the fitting procedure were compared: the mean X and Y root mean square error was 30 pm; and the mean RMS Z error was 0.798 pm. These errors are negligible compared with the shot-noise limited positional accuracy.

2.3 Positional accuracy

As shown in section 1.3, Thompson et al [6] derived a theoretical estimate for the positional accuracy in 2-dimensional single particle imaging in terms of PSF width σ_{xy}, total number of photons in peak N_p, background b and pixel size a. In order to compare our results with the 2D prediction, simulations were restricted to just 1 slice, and so 2D images were generated. Many simulations were made over a range of values for background noise b and number of photons collected N_p, and the results were compared with the predictions by Thompson (see figure 2.5). The positional

accuracy was found to range from 4.5 ± 0.2nm for a bright peak with a high signal-to-noise (SNR) of 500, to 18.5 ± 0.6nm for a dimmer peak with a low SNR of 10. Conditions typical is our set-up are $N_p \sim 1000$ in a single slice and a background of $b \sim 0.5$. This corresponds to single slice 2D positional accuracy of 11.0 ± 0.7nm.

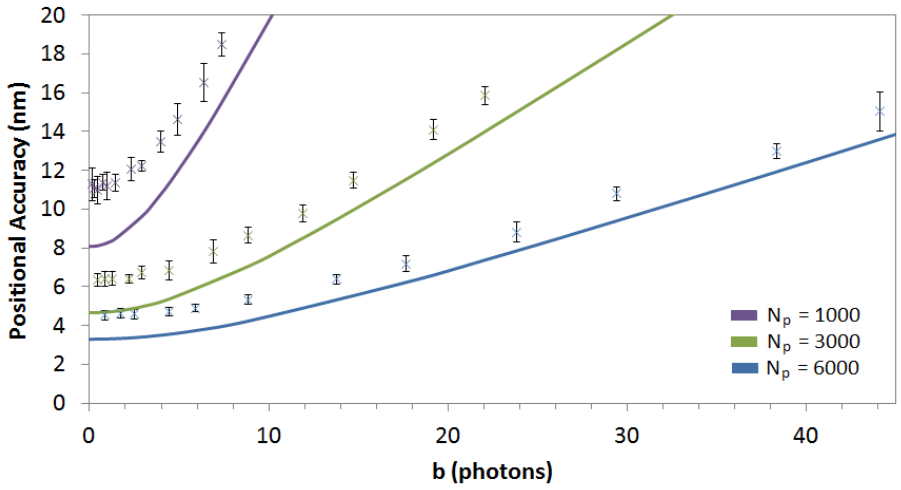

Figure 2.5: 2-dimensional positional accuracy. *The theoretical predictions (solid lines) according to equation 1.3 are compared with measurements on simulated images (points), for three values of the total number of photons N_p. Each measurement point is the average positional accuracy from 10 separate sets of 200 images - and the error bars are the standard deviation on those 10 values (in total, 2000 images per point). The measured values are consistently higher than the theoretical estimates, as in Thomson et al [6]*

Compared to the theoretical predictions, the measured positional accuracy was between 25% and 30% higher. This offset is in agreement with the findings of Thompson et al: they reported that in the ranges they investigated their measured values for the positional accuracy of both real and simulated images were consistently around 30% higher than their theoretical estimates. An offset to the formula was also found experimentally by van der Broek et al [3], and was suggested to be due either to diffusion of the GNR between acquisition of slices, or due to the point spread function perhaps not being Gaussian. However, the results from simulation, both in this study, and in the work of Thompson, suggest this is not the case; in the simulation we do not have movement between acquisitions, and the point spread function generated is indeed Gaussian - yet the offset remains. Thompson suggested the offset was due to their fitting procedures not taking into account shot noise - which could be the case here too.

A theoretical estimate for the positional accuracy in 3-dimensional single particle imaging was not found in literature, or been made yet, to our knowledge. As outlined in the introduction, our hypothesis is that as there are more photons collected in the 3D image, the positional accuracy will be better. 2-dimensional and 3-dimensional images were compared, as shown in figure 2.6. The 3D images were created by adding 4 extra slices with spacing of 1.5 µm (2 below and 2 above the single slice simulations), keeping all other settings unchanged. This resulted in about 10% more collected photons, and the positional accuracy improved by on average 25%. The accuracy depends strongly on the number of photons received, which itself in 3D microscopy depends strongly on the separation between the 2D slices. Closer separations result in more photons and so higher accuracy. For example, typical experimental slice separations of 0.5 µm and 1.5 µm, corresponding to number of photons $N_p \sim 3000$ and ~ 1000 received respectively, result in accuracies of 5.2 ± 0.3nm and 8.9 ± 0.6nm.

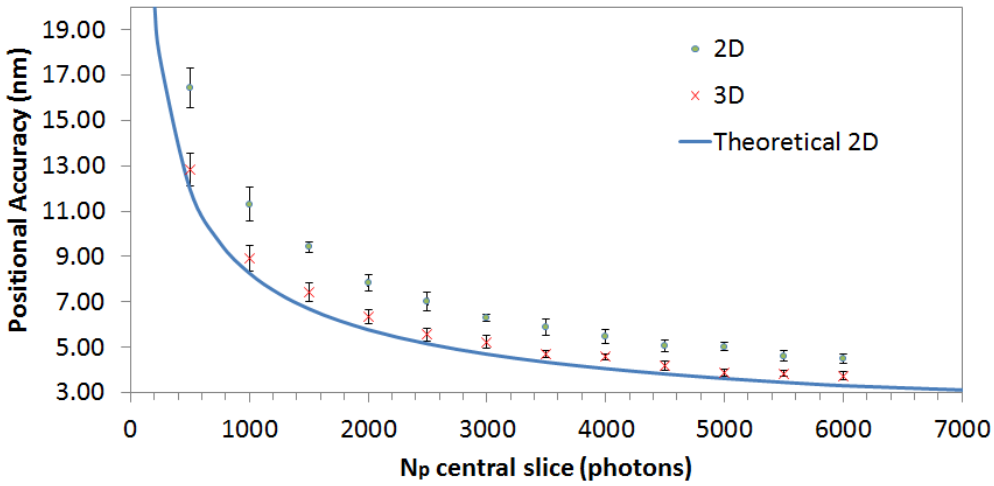

Figure 2.6: 2D and 3D positional accuracy. *The graph compares results from simulations in 2D and 3D, and the 2D theoretical estimate from Thompson [6]. 3D images involve more collected or simulated slices through the PSF, which increase the number of photons collected and increases the positional accuracy. The 2D images are based on N_p collected photons in a single slice. The 3D (5-slice) images are based on N_p* ***photons in the central slice****, with the other slices adding to the total number of photons, and so to the accuracy. In all simulations, Poisson-distributed photon noise is simulated, so the number of photons per simulation is not fixed. The same background noise is used in both cases: $b = 1$.*

2.4 Characterising particle behaviour

Next we investigated the uncertainty in extracting movement information from trajectories, using MSD plots (as outlined in section 1.4). As MSD plots only require a set of co-ordinates, it is not required to generate and analyse images. As a significant amount of the time required for simulations was due to these steps, there was a motivation to bypass them. Using equation 1.3, and the results of the previous sections, we could determine the positional accuracy of the microscope given a measurement of the background b and total number of photons per image N_p. Given a simulated diffusive trajectory, we added Gaussian noise with the width equal to the positional accuracy. This bypassing step is outlined in the following schematic:

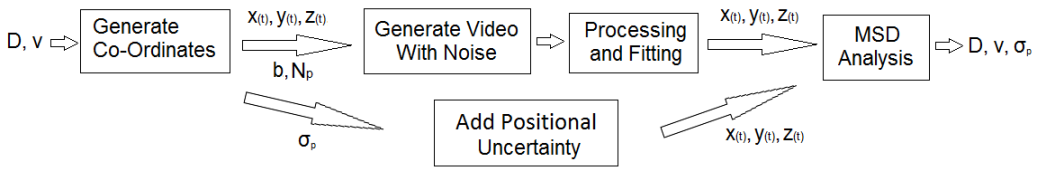

Figure 2.7: Scheme for steps involved in full simulation, and for simulations bypassing images generation. *Simulation so far have been made in the following way: trajectory co-ordinates were generated, images of those trajectories were created, and then the positions were extracted by fitting the GNRs in those images. The extracted co-ordinates do not match the original co-ordinates due to the finite positional accuracy of the fitting procedure. Now that we know the positional accuracy, we can skip the image generation step by adding uncertainty directly to the trajectory co-ordinates.*

To validate the approach, the 2D positional accuracy results given in figure 2.5 were reproduced using the new method: a good agreement was found, as shown in figure 2.8.

Version of March 22, 2016– Created March 22, 2016 - 11:05

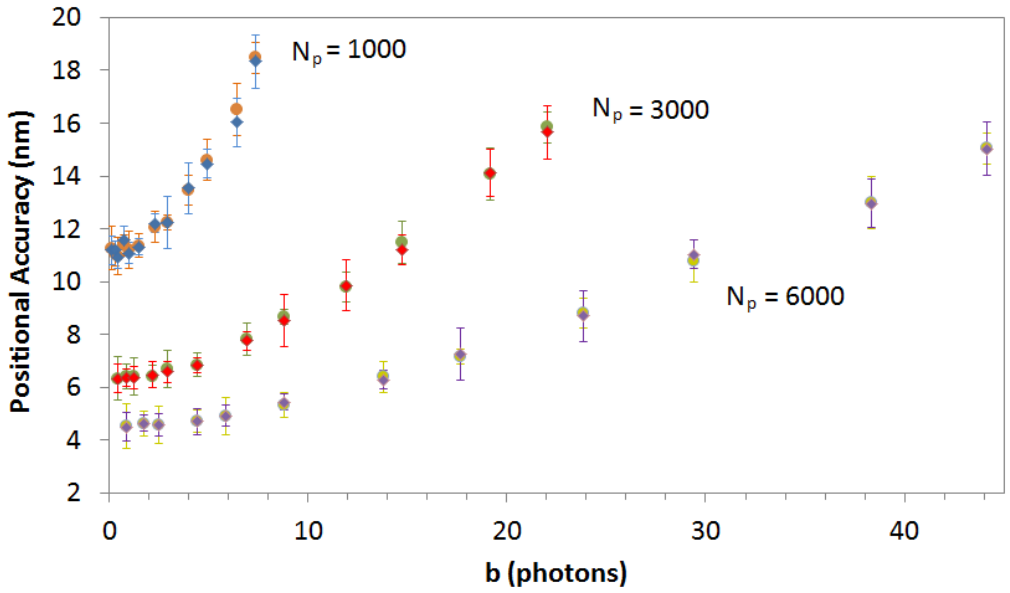

Figure 2.8: Validation of simulating without creating images. *The method of directly adding uncertainty into generated co-ordinates is tested: circles correspond to results from simulations using images (from figure 2.5) and diamonds correspond to results from simulations bypassing image generation. Each point is the average accuracy from 10 sets of 200 simulations, error bars are the standard deviation on those 10 sets. Three cases of total photon number N_p were tested.*

2.4.1 Statistical uncertainty extracting behaviour properties from MSD plots

As outlined in section 1.4, there is an inherent statistical uncertainty in extracting parameters of motion from an MSD plot, resulting in an expected relative error δ_D:

$$\delta_D = \frac{(D_{Detected} - D_{Actual})}{D_{Detected}} \tag{2.3}$$

Qian et al [7] derived a theoretical upper estimate of this error, dependant on the length of trajectory N, and number of fitting points n used in the MSD plot, stated again here:

$$\delta_{D_{max}} = \pm\sqrt{\frac{2}{3}}\sqrt{\frac{n}{N-n}} \tag{2.4}$$

Their derivation is purely statistical, assuming perfect positional accuracy, but is a good approximation at high positional accuracy. The formula states that using $n = 2$ points in an MSD plot minimises the *maximum* relative error - however it is unclear if this minimises the *average* relative error. We tested it at two values of diffusion coefficient relevant to our experimental set-up. Purely diffusive trajectories of fixed diffusion coefficient D_{Actual} were simulated, and the relative error was assessed over a range of n for two values of positional accuracy σ_p, as shown in figure 2.9. Both at $\sigma_p = 10\,\text{nm}$ and $\sigma_p = 200\,\text{nm}$, the bounds were seen to be a good fit and $n = 2$ was confirmed to give the lowest relative error, though there was a bias to underestimate the diffusion coefficient.

Figure 2.9: (Next page) Relative error in extracting D, as a function of number of fitting points n. *These graph show that the upper estimate [red dashed line] of expected relative error when extracting D from MSD plots (See equation 2.4, from Qian et al [7]) is a good bound for the range of positional accuracy expected for our microscope. For each graph, 100 purely diffusive ($D = 0.5\,\mu\text{m}^2\,\text{s}^{-1}$) trajectories of length $N = 200$ were generated, and D was extracted by fitting MSD plots made over a range of fitting points n. The results are shown using box-diagrams: the centre of the box is the median, the edges are each a standard deviation, the whiskers are the 10th and 90th percentiles, and points outside those bounds are crosses. Both plots show a bias for underestimating the diffusion coefficient.*

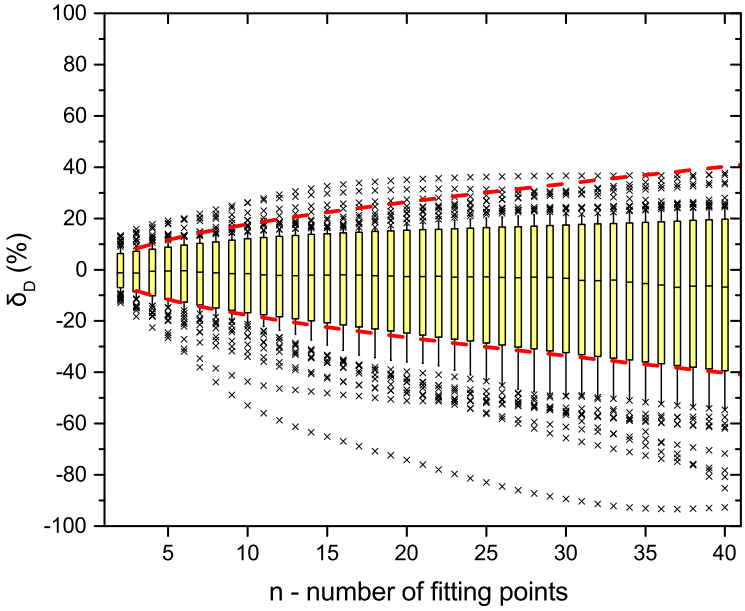

(a) $\sigma_p = 10\,\mathrm{nm}$

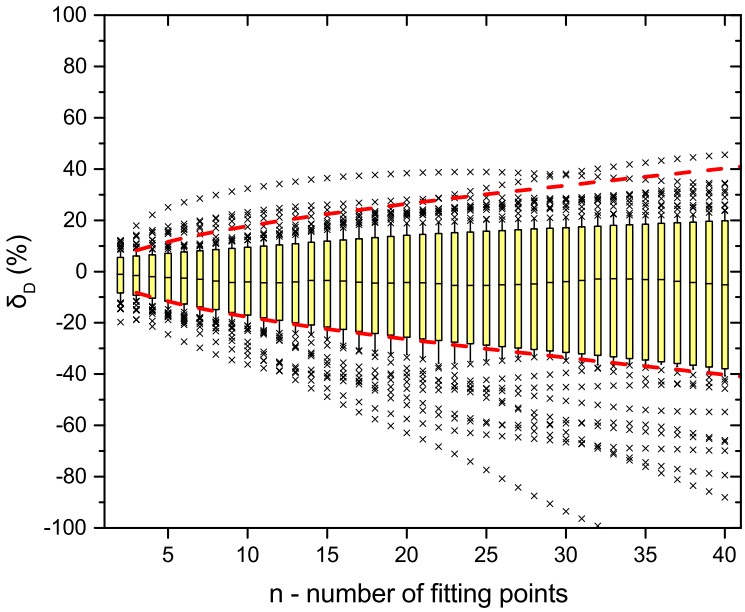

(b) $\sigma_p = 200\,\mathrm{nm}$

2.4.2 Optimising the accuracy of extracting behaviour properties from MSD plots

According to Michalet [8], who extended the work of Qian, and considered the effect of a positional accuracy, there is a best number of fitting points n in an MSD plot, that optimises the accuracy of extracted parameters. This is dependent on the positional accuracy, frequency of measurement, length of trace and parameters being extracted (either velocity, diffusion coefficient, or positional accuracy). Mitchalet numerically determined the optimal value for a range of x (reduced localization error, dimensionless, see section 1.4) from $0.01 - 1000$ (this includes our entire range of expected experimental conditions) for extracting either the positional accuracy, or the diffusion constant. He found that the difference in n_{optimal} in the two cases was negligible, and could be approximated by the relation:

$$n_{\text{optimal}} = 2 + 2.3x^{0.52} \tag{2.5}$$

Due to the high positional accuracy of our microscope, we would expect $x << 1$ for most experimental conditions over the range of D and N expected. This was verified numerically, shown in figure 2.10: all MSD plots were fitted with equation 1.5 with v set to zero, assuming purely diffusive motion, in line with the work from Michalet. The values of $n_{optimal}$ given by equation 2.5 were found to be accurate, particularly at high positional accuracy, indicated by dashed lines in figure 2.10. As shown in figure 2.10a, at $\sigma_p = 10\,\text{nm}$, for all values of D, $n_{\text{optimal}} = 2$ was predicted and measured. As shown in figure 2.10b, for $\sigma_p = 200\,\text{nm}$ the predicted values were, rounded to the nearest integer, $7, 3, 2$ and the measured values were $7, 2, 2$ for diffusion coefficients D of 0.01, 0.5 and 1 $\mu\text{m}^2\,\text{s}^{-1}$ respectively. Finally, as shown in 2.10c, for $\sigma_p = 2000\,\text{nm}$ the predicted values were $7, 9, 54$ and the measured values were $6, 7, 48$ over the same range of D.

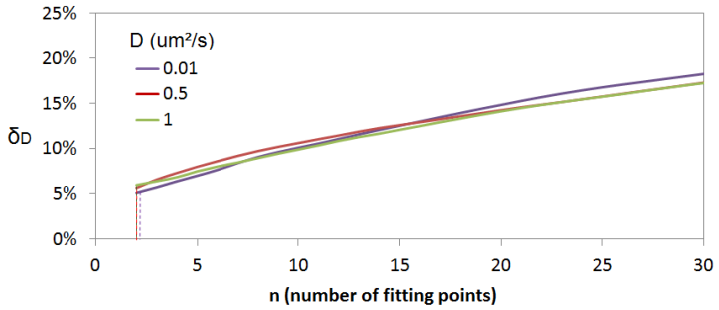

(a) $\sigma_p = 10\,\mathrm{nm}$

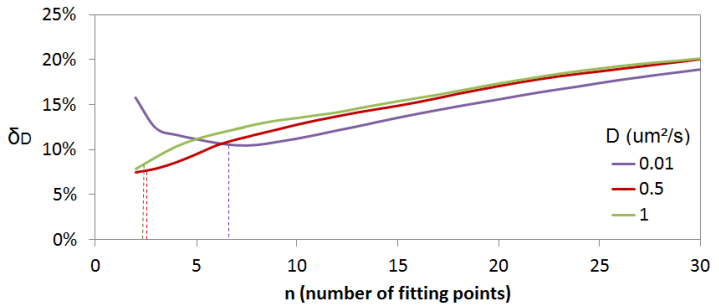

(b) $\sigma_p = 200\,\mathrm{nm}$

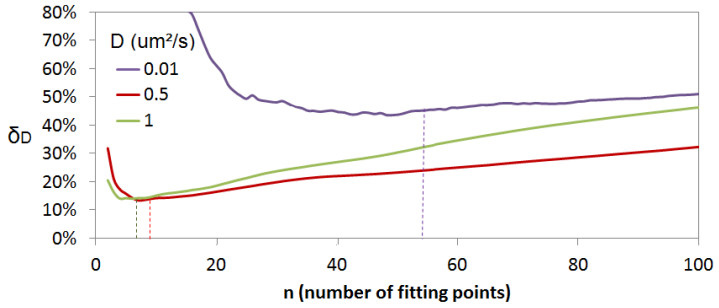

(c) $\sigma_p = 2000\,\mathrm{nm}$

Figure 2.10: Optimal number of fitting points to reduce expected error. *Purely diffusive trajectories were simulated for three values of σ_p, each for three diffusion coefficient D values (0.01, 0.5 and 1 $\mu m^2\,s^{-1}$). D was extracted from MSD plots made from a varying number of fitting points n, and the average relative error of its calculation over 100 simulations for each combination of parameters was plotted. The predicted $n_{optimal}$ for each curve [16] is marked by vertical dashed lines. The predictions were found to be accurate, particularly at high positional accuracy.*

As outlined in section 1.4, movement parameters are extracted from fitting MSD plots with the equation:

$$MSD(\tau) = 2dD\tau + v^2\tau^2 + 2d\sigma_p^2 \tag{2.6}$$

In this formula, τ is the delay and d is the number of dimensions of the system. If any one of the variables, diffusion coefficient D, velocity v or positional accuracy σ_p is already known, by fixing it the fit will be improved, and the relative error in extracting other parameters should be reduced. As the positional accuracy can be calculated from the Gaussian peak intensity and PSF width, we tested using simulations to verify that fixing it did reduce the relative error. The results shown in figure 2.11 indicate an average reduction of relative error δ_D for short trajectories ($N = 20$) of 6.84%, medium-length trajectories ($N = 200$), 1.81%, and for long trajectories ($N = 2000$), 0.64%.

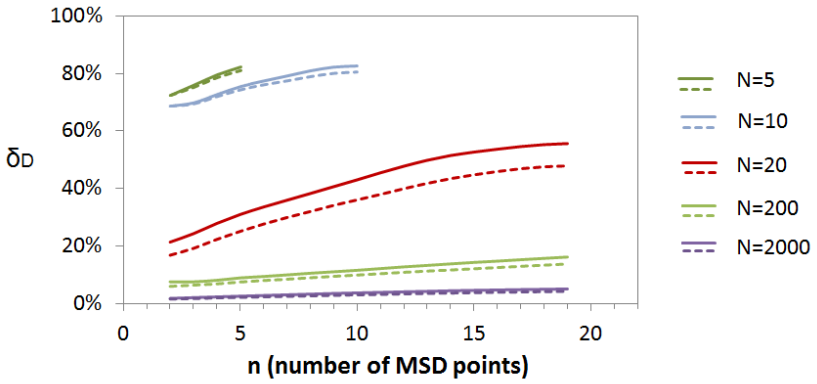

Figure 2.11: Fixing the positional accuracy σ_p reduces the relative error δ_D in extracting the diffusion coefficient. *The solid lines represent the case where both σ_p and D are fitted, and only $v = 0\,\mathrm{m\,s^{-1}}$ is fixed. The dashed lines show the case where only D is fitted and and both the other parameters are fixed: $v = 0\,\mathrm{m\,s^{-1}}$ and $\sigma_p = 10\,\mathrm{nm}$. 100 purely diffusive trajectories with $D = 1\,\mu\mathrm{m^2\,s^{-1}}$ and $\sigma_p = 10\,\mathrm{nm}$ were simulated and analysed, for each length in a range between $N = 5$ and $N = 2000$. The resulting MSD plots were fit with equation 2.6 using a range of fitting points n. $n_{optimal}$ is not affected by which parameters are fixed. (The test was repeated for $D = 0.5\,\mu\mathrm{m^2\,s^{-1}}$ and $D = 0.1\,\mu\mathrm{m^2\,s^{-1}}$, shown in the appendix in figure 4.1)*

Next we investigated the relative error expected when extracting the velocity of a purely ballistic particle from MSD plots, defined as $\delta_v = (v_{Detected} - v_{Actual})/v_{Detected}$. We would expect that extraction from longer trajectories should be more accurate, as there is simply more data to fit. Secondly, assuming that the direction of movement is constant, as this is not a stochastic process, we expect a minimal uncertainty, due to the finite positional accuracy. Simulated trajectories were analysed of varying lengths and varying GNR velocities, shown on the next page in figures 2.12 and 2.13 and also in the appendix in figure 4.2.

As expected, it was found that the accuracy scales with trajectory length (compare figures 2.12 and 4.2, in which the only variable changed is the trajectory length). It was also found that as number of fitting points n was increased, a minimal plateau was reached at around $n = 0.4N$. n_{optimal} was about $0.7N$, and after about $n = 0.8N$, the accuracy began to decrease again. For a high velocity GNR, as shown in figure 2.13, the choice of n is not really important; for $v \geq 0.5\,\mu\text{m}\,\text{s}^{-1}$, all tested trajectory lengths N (20, 200, 2000) and any choice n returns the set v with on average under 0.1% relative error. If accuracy in extracting low velocities is required, then the choice of n does have an effect - particularly for shorter trajectories - and setting n inside the range indicated above can improve accuracy significantly, see figure 2.12. This is because at low velocity, the movement is comparable to the positional uncertainty.

The MSD plots were fitted with equation 1.5, which is a function of σ_p, D, and v. The effect on the accuracy of fitting the other parameters was investigated and is also shown in figures 2.12 and 2.13 and 4.2. Fixing D alone gives the largest improvement (from green to red line) - although this is not possible in real measurements. Surprisingly fitting just v is slightly less accurate than fitting σ_p and v - this indicates that perhaps the fitting procedure could be improved.

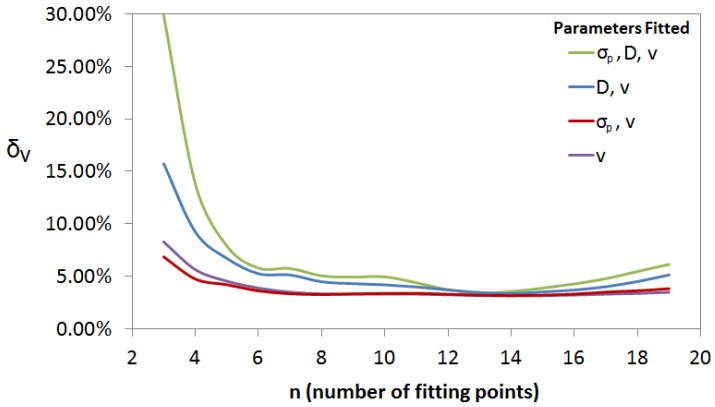

Figure 2.12: Optimal number of fitting points $n_{optimal}$ for slow ballistic particles ($v = 0.01\,\mu\mathrm{m\,s^{-1}}$). *The graph shows that for low velocity particles, regardless of which parameters are fixed and which fitted, that relative error reaches a plateau around 5% after about 6 points - if fewer points are used, the relative error increases sharply. Each point on each curve is the average relative error from 100 simulated trajectories of length $N = 20$, with positional accuracy $\sigma_p = 10\,\mathrm{nm}$. Each curve corresponds to fitting the parameters labelled, and fixing the others to their set values.*

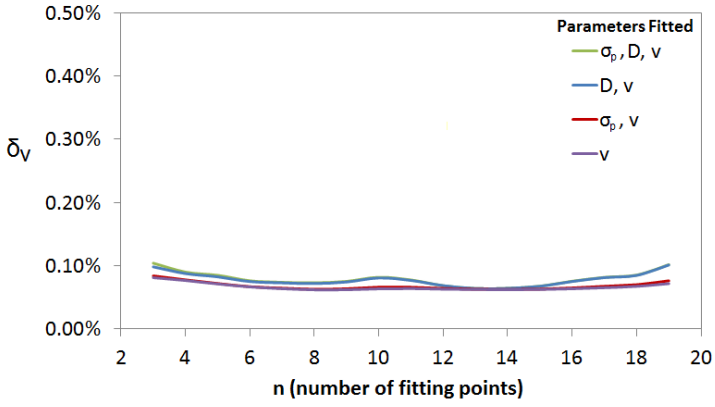

Figure 2.13: Optimal number of fitting points $n_{optimal}$ for fast ballistic particles ($v = 0.5\,\mu\mathrm{m\,s^{-1}}$). *The graph shows that for high velocity particles, the accuracy of v is always very high. Each point on each curve is the average relative error from 100 simulated trajectories of length $N = 20$, with positional accuracy $\sigma_p = 10\,\mathrm{nm}$. Each curve corresponds to fitting the parameters labelled, and fixing the others to their set values.*

2.4.3 Detecting behaviour transitions

In real experiments it is quite common that a particle undergoes a change in behaviour, for example from free diffusion to ballistic motion. In this section we investigate detecting this quantitatively using a statistical method to identify the point in a trajectory that such changes occur. Student's t-test compares two populations and evaluates how well they can be described by the same distribution, using sample mean and sample variances; it gives a likeliness value between $0 \geq p \geq 1$ that two samples are from the same distribution. Here we use a variant of Student's t-test for populations of unequal variances, known as Welsh's test [17]. This test is known to be more accurate when samples are of unequal variances, which is the case here since the variances of the velocity and diffusion coefficients distributions vary. The Welsh test involves calculating the t-statistic and approximating the pooled degrees of freedom ν as the following:

$$t = \frac{\overline{X}_1 - \overline{X}_2}{\sqrt{\frac{\sigma_1^2}{N_s} + \frac{\sigma_2^2}{N_s}}} \tag{2.7}$$

$$\nu \approx \frac{\left(\sigma_1^2 + \sigma_2^2\right)^2}{(\sigma_1^4 + \sigma_2^4)/(N_s - 1)} \tag{2.8}$$

t and ν are calculated using the sample means $\overline{X}_1$ and $\overline{X}_2$, sample standard deviations σ_1 and σ_2, and sample size N_s. The likelihood of the samples being described by the same distribution is then calculated using these values in the t-distribution probability density function [17], in our case we used Excel's built-in function for this.

$$p(t, \nu) = \frac{\Gamma(\frac{\nu+1}{2})}{\sqrt{\nu\pi}\,\Gamma(\frac{\nu}{2})} \left(1 + \frac{t^2}{\nu}\right)^{-\frac{\nu+1}{2}} \tag{2.9}$$

To use the likeliness value to indicate a transition at a time t, two samples of size N_s are taken at each side of t from data characterising the mode of action. p is then interpreted as the likelihood that the two samples are of the same mode of action; a low value indicates transition.

Two trajectories were simulated and analysed using Welsh's test: each starts with a period of diffusion followed by a period of ballistic motion, followed by a final period of diffusion. Typical experimental conditions were used: $D = 0.5\,\mu\text{m}^2\,\text{s}^{-1}$, $v = 0.5\,\mu\text{m}\,\text{s}^{-1}$ and the positional accuracy was $\sigma_p = 10\,\text{nm}$. The first, 'clear' trajectory has a ballistic period of 50s,

and the second 'less clear', a period of 25s. The simulated trajectories were analysed with MSD plots to extract the values of D and v as in typical experimental procedure. To get time-series values for v and D, the trajectory of length N was analysed in windows of length N_w (Note that the window length N_w and sample length N_s need not be the same). To maximise the accuracy of the extracted values (as outlined in section 2.4.2), D was extracted from MSD plots made from $n = 2$ fitting points, and v was extracted from MSD plots made from $n = 0.7 \times N_w$ fitting points.

For each trajectory, the test was carried out for three different values of the window length N_w: 5, 15 and 30 seconds. Longer windows provide more data for MSD plots, and so more accurate values for D and v. However, this must be balanced with the fact that longer windows will be more likely to include multiple modes of action, and so blur the boundaries in the diffusion and velocity time-series. We carried out Welsh's test on time-series of the diffusion coefficient D and the velocity v:

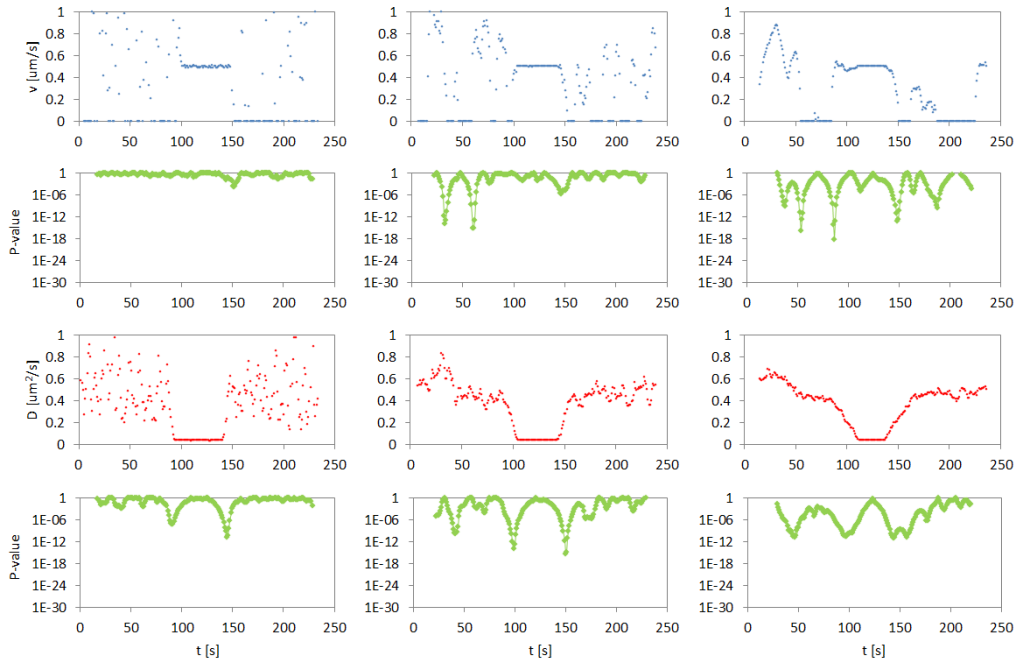

Figure 2.14: Comparison of window sizes and data source for Welsh's test. *Left to right: window sizes N_w of 5, 15 and 30. Top to bottom: time series of velocity, P-value calculated using that, diffusion coefficient, and P-value calculated using that. The trajectory analysed is the 'clear' transition described in text, with transitions at 100s and 150s. The minima in the P-value should indicate transitions. The sample size in all cases is $N_s = 15$. Note that the P-value plots are logarithmic.*

Figure 2.4.3 shows the p-value time-series calculated using diffusion coefficient data is more useful than the series calculated using velocity data. For the velocity-calculated p-values, the minima do not coincide with transition points. The extracted velocity varies widely, particularly for small window size N_w. This is because when there are few points in an MSD plot, linear and quadratic curves fit similarly well, so the line of best fit does not consistently set the quadratic term to zero: the Welsh test is not at fault. Nevertheless, from here on we shall calculate p-values using the diffusion data. Figure 2.4.3 shows that p-value time-series created using smaller window lengths indicates transitions more clearly. The transitions are clearest when the corresponding minima in the plots are many magnitudes of order lower than other 'false' minima. In the series created with windows of size $N_w = 30$, the true and 'false' minima are not easily distinguished.

Next, we tested three different values for the sample size N_s: 5, 15 and 30. Larger samples provide more data, so we would expect the test to return higher and lower p-values, and so identify transitions better. However, if a period of motion is shorter than the sample size, the sample will unavoidably include multiple modes of action, and the transition points will be less distinct. To detect short transient modes of action then, smaller samples are better. We must make a compromise: we want the smallest sample size possible that still distinctly indicates transitions. We found, as expected the larger samples did result in much lower p-values for the transitions, and so much clearer indications:

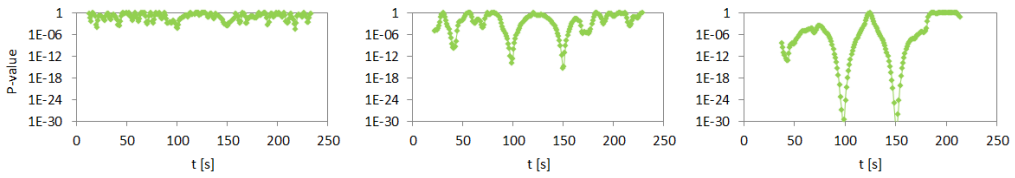

Figure 2.15: Effect of Welsh's test sample size on transition p-value. *The graphs show the p-value time series resulting from Welsh's test performed on the 'clear' trajectory described in the text, with transitions at 100s and 150s, using different sample sizes. Left-to-right, the sample size N_s are: 5,15 and 30. All the tests were carried out on diffusion coefficient data extracted from MSD plots, using windows of size $N_w = 15$. Note that the P-value plots are logarithmic.*

In summary, the p-values should be calculated using the diffusion data, the window length N_w should be small, and the sample size N_s should be large. Figures 2.16 and 2.17 show the two trajectories studied, and the combinations of N_w and N_s giving clearest indications of transitions.

Version of March 22, 2016– Created March 22, 2016 - 11:05

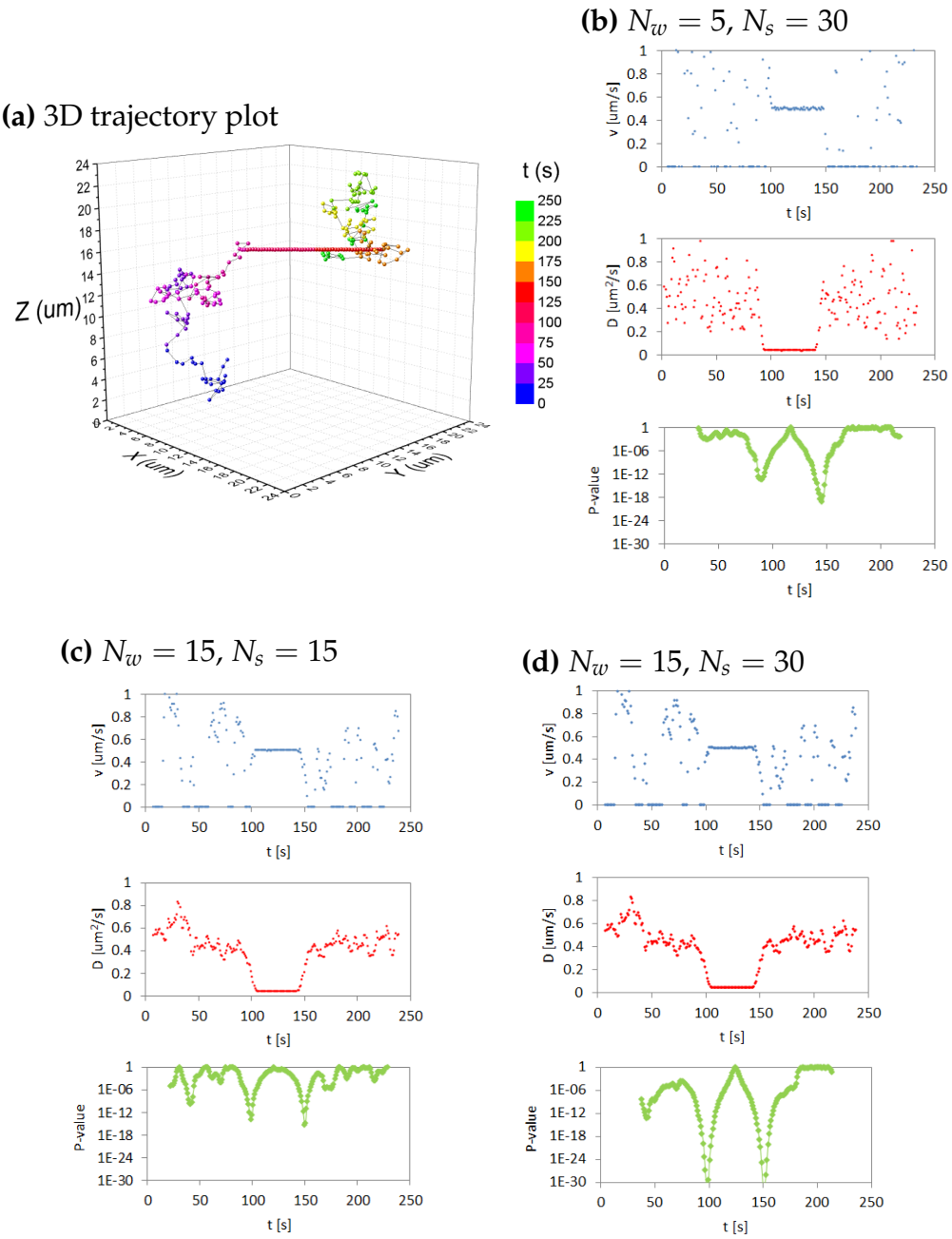

Figure 2.16: Analysis of a mixed trajectory with "clear" transitions. ***(a)*** *A plot of the trajectory: two* 100 s *periods of diffusive motion ($D = 0.5\,\mu m^2\,s^{-1}$), separated by a* 50 s *period of ballistic motion ($v = 0.5\,\mu m\,s^{-1}$).* ***(b), (c)*** *and* ***(d)*** *show for different combinations of window length N_w and sample size N_s, time-series of D and v extracted from MSD plots, and of the P-value resulting from Welsh's test. In all cases the P-values are calculated using the diffusion coefficient time-series. Note that the P-value plot is logarithmic.*

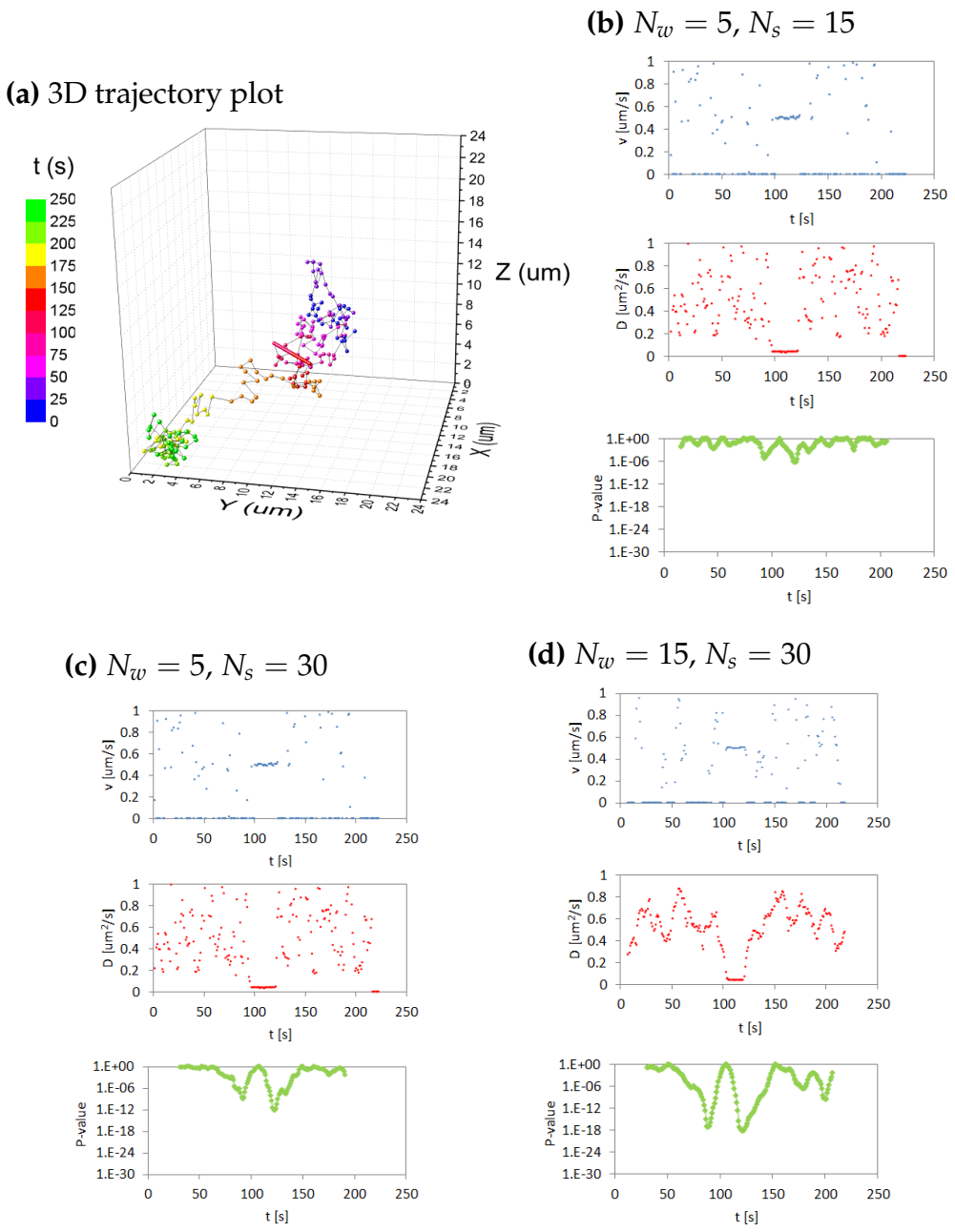

Figure 2.17: Analysis of a mixed trajectory with "less clear" transitions. ***(a)*** *A plot of the trajectory: two* 100 s *periods of diffusive motion (*$D = 0.5\,\mu\mathrm{m}^2\,\mathrm{s}^{-1}$*), separated by a* 25 s *period of ballistic motion (*$v = 0.5\,\mu\mathrm{m}\,\mathrm{s}^{-1}$*).* ***(b), (c)*** *and* ***(d)*** *show for different combinations of window length* N_w *and sample size* N_s*, time-series of* D *and* v *extracted from MSD plots, and of the P-value resulting from Welsh's test. In all cases the P-values are calculated using the diffusion coefficient time-series. Note that the P-value plot is logarithmic.*

2.5 Movement between slices

Experimentally, in a 3D stack there is a lag of 0.1 s between slices due to the finite time required by the camera to collect photons. In simulations created so far in this work, movement has been considered to occur entirely between stacks, instead of between the slices within those stacks. However, we would expect the movement between slices to distort the Gaussian shape of the PSF, as illustrated in figure 2.18, potentially making the fit and position inferred less precise.

Figure 2.18: Movement between slices. *The three stacks on the left show the actual point spread function of a particle across three slices, at three successive points in time. The particle is centred on the middle slices and is moving in the XY plane. The darkened slices are those actually acquired up by the microscope, due to its lag. The subsequent distorted Gaussian can be seen in the stack produced on the right.*

To determine the impact of this effect on the results, diffusive movement was simulated between slices, and the effect on the positional accuracy was found to be substantial, especially at high rates of diffusion. Previous results, shown in figure 2.6, determined the 3D x-y positional accuracy in typical experimental conditions to be about 8.9 ± 0.6nm (z-separation of 1.5 µm). As shown in figure 2.19, for the same experimental conditions, the x-y positional accuracy for slow diffusive GNRs ($D = 0.01\,\mu m^2\,s^{-1}$) was 9.5 ± 0.6nm, and for the fastest diffusive GNRs tested ($D = 0.5\,\mu m^2\,s^{-1}$), it was an order of magnitude worse at 143.0 ± 8.4nm. In the z-plane, the accuracy was lower at 22.1 ± 1.2nm and 243.1 ± 34.3nm respectively. Simulations were made with and without noise, and it was found that the effect of noise on positional accuracy is small compared with the effect due to movement between slices.

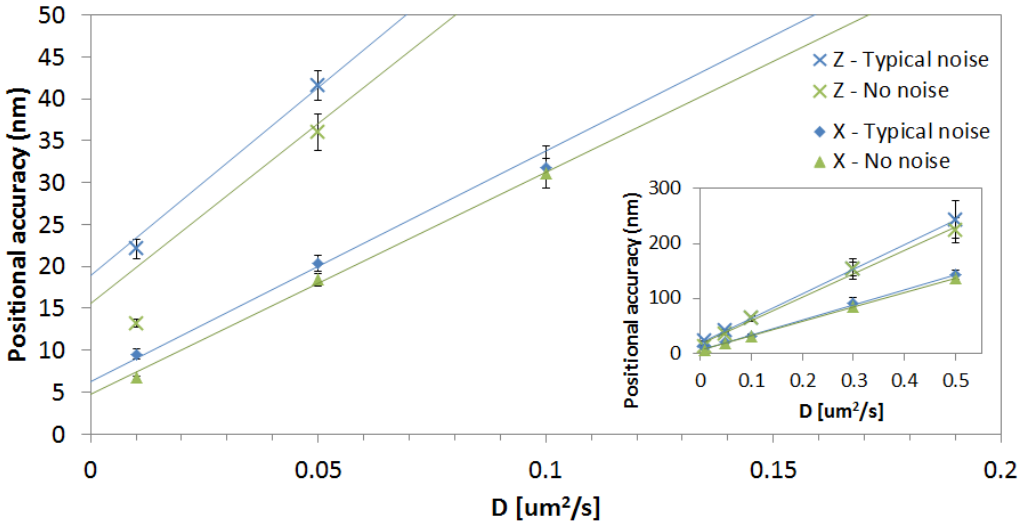

Figure 2.19: Effect of diffusive movement between slices on the positional accuracy. *This graph shows the resulting average positional accuracy on simulated GNRs, whose diffusive movement occurs between each 2D slice (The full 3D images are stacks of 2D images). The main panel shows the experimentally relevant range of diffusion coefficients, and the inset extends this. Each point represents the average of 1000 simulated trajectories. Trajectories were created with and without background noise - which is Gaussian with width $b = 0.5$ photons. The separation between slices is* 1.5 µm*, and the total number of photons per GNR is about* 1150*, but varies due to the implementation of photon-noise. Lines of best fit have been imposed to illustrate the linear relationship.*

As reported previously by van den Broek et al [3], the fastest diffusive movement for GNRs in cells was found to be $D = 0.1\,\mu m^2\,s^{-1}$. At this rate of diffusion, our results are an x-y positional accuracy of 31.8 ± 2.5nm and z positional accuracy of 65.3 ± 3.5nm. This is an order of magnitude higher than for stationary GNRs, and is

Figure 2.19 indicates a linear relation between the positional accuracy and the diffusion coefficient. However, before concluding the relation is strictly linear, further work should be done at lower values for the diffusion coefficient. For example, the fit for the x-y accuracy with typical noise is $\sigma_p = 6.3 \sim 275D$ (same units as for plot). This would indicate that in the case of no diffusive movement, in typical experimental conditions, with z-separation of 1.5 µm, the positional accuracy should be 6.3 nm. However, we already found in section 2.3 that this was 8.9 ± 0.6nm. This suggests that the relationship is not linear at low D, that it levels off, similarly to figure 2.5.

Chapter 3

Discussion

In this study we characterised the accuracy and limitations of using gold nanorods (GNRs) in our two-photon scanning microscope, by analysing the tracking of simulated GNRs. We took real two-photon luminescence images of GNRs captured by the microscope, and fit the intensity distributions due to the photons as Gaussians, which is known to be a good approximation [14]. By fitting the distribution, we determined the average values and ranges of the widths σ_z, σ_x, and σ_y, and total number of photon N_p. We simulated two-photon luminescence images of GNRs with these properties, which compared well with the real images.

The 3D positions of GNRS in stacked images are determined by fitting Gaussian profiles to the photon intensity distributions. The positional accuracy of this 'super-resolution' method is not known. We numerically determined the positional accuracy by fitting the intensity distributions due to stationary simulated GNRs, and comparing the set co-ordinates and fitted co-ordinates. We first tested this on 2D images, and our results matched the previous work of Thompson et al [6]. The positional accuracy was dependant on the number of photons received: for example, in the range relevant to our experimental set-up, with a Gaussian background noise of width $b = 0.5$ photons, ~ 1000 captured photons gives a 2D positional accuracy of 11.0 ± 0.7nm. We hypothesised that the positional accuracy in the xy-plane would be better in 3D due to the increase in number of photons. We verified this numerically, and found the accuracy was increased by on average 26%. In typical experimental conditions the accuracy was numerically determined to range between 5.2 ± 0.3nm and 8.9 ± 0.6nm, corresponding to Z-separations of 0.5 µm and 1.5 µm, which each on average capture ~ 1000 and ~ 3000 total photons respectively. Experimentally there is a trade-off concerning separation distance between

slices: short separation increases number of photons and so accuracy, but decreases the depth of the sample probed. We have shown that for example, if an accuracy of 8 nm is sufficient, for positioning stationary particles, the larger separation can be used.

Next we simulated GNRs with diffusive trajectories and numerically determined the relative error in extracting the diffusion coefficient from MSD plots. Our results agreed with the theoretical maximum relative error predicted by Qian [7]. We found however, that there is a bias to underestimating the diffusion coefficient, shown in figure 2.9, which should be investigated.

The accuracy of extracting values of variables of motion from MSD plots is dependent on the accuracy of the fit. Mitchalet [8] derived a theoretical prediction for the optimal number of points to use. We numerically tested the prediction, and our results agreed over a range of diffusion coefficients, positional accuracies and velocities. We found that at high positional accuracy ($< 10\,\text{nm}$), for diffusive trajectories, using only 2 points gives the best accuracy for the diffusion coefficient. The relative error extracting the velocity from fast ballistic trajectories ($v = 0.5\,\mu\text{m}\,\text{s}^{-1}$) was always low ($\sim 0.1\%$) regardless of choice of n. On the other hand, we found that for slow ballistic trajectories $v = 0.01\,\mu\text{m}\,\text{s}^{-1}$, that using less than $n = 0.4N$ points results in large errors, ($< 10\%$), and that $n = 0.7N$ gives the highest accuracy (see figure 2.12). The high relative error at low velocity is due to the the ballistic movement being less distinguishable from the apparent movement due to the limited positional accuracy. In summary the number of points to use in an MSD plot depends on the which variable is to be extracted, and what value is expected for it: if only the diffusive motion is of interest, use only 2 points; if interested in slow ballistic movement, use a high number $n > 0.4N$; if interested in fast ballistic movement, the choice of n does not matter.

The positional accuracy can be calculated from the Gaussian fit on the 3D PSF, so we can fix that parameter when fitting MSD plots. We numerically determined that this does improve the fit and the accuracy of extracting the diffusion coefficient of diffusive trajectories, and the velocity from ballistic trajectories. The shorter the trajectory the greater the improvement: the average on long $N = 2000$ trajectories was 0.6%, on $N = 200$ it was 1.7% and for short trajectories $N = 20$ it was 6.5%. The improvement in accuracy on the short trajectories is significant, so for these the positional accuracy should be determined and fit.

We investigated using Welsh's test to detect transitions in particle behaviour. The test compares two samples of data and determines the likeliness (p-value) that they are from the same distribution. By performing the

test on diffusion coefficient or velocity time-series for a particle trajectory, we can identify the transitions as the minima of the p-value. However, we found that only the diffusion coefficient data reliably indicated transitions. To get time-series for the diffusion coefficient and velocity throughout a trajectory, we fit MSD plots on windows of length N_w across the trajectory. We tested three lengths of window (5, 15 and 30 s), and found that using the shorter windows (5 and 15 s) resulted in Welsh's test more clearly indicating transitions: the smaller the window, the more prominent the minima corresponding to the transitions. Welsh's test compares two samples each of size N_s taken either side of time t in a trajectory. We tested three sample sizes (5, 15 and 30 s), and found that the larger sample size (15 and 30 s) results in clearer indications of transitions. The larger the sample size, the smoother the p-value changes, making the minima corresponding to the transitions clearer. In summary, Welsh's test should be carried out on diffusion coefficient data, extracted from MSD plots calculated on small windows N_w, using large sample sizes N_s. Next, the conclusion drawn here for N_s and N_w should be tested on a range of different trajectories and transitions, with a range of values for the diffusion coefficient and velocity.

Finally, we found that the diffusive movement of a particle has a large negative impact on the accuracy of Gaussian fit of the PSF. The 3D image of the GNR is made of a stack of 2D slices collected by the microscope with a delay between slices of 0.1 s. This means that the observed PSF will be distorted, more so for faster or more diffusive movement. We altered our simulation for movement to occur between slices, not only between stacks, and numerically determined the resulting positional accuracy over a range of diffusion coefficients. The fastest diffusion rate for GNRs observed in cells with our set-up was $D = 0.1\,\mu m^2\,s^{-1}$ [3]. With a z-separation between slices of 1.5 µm we would then expect x-y positional accuracy of 31.8 ± 2.5nm. Movement between slices therefore dominates our positional accuracy at higher diffusive rates: the technique only has < 10 nm for the slowest particles, which is a severe limitation compared with other techniques. To improve the positional accuracy, we could try to improve the fit of the particle PSFs, for example by using non-Gaussian distributions: Titus et al have shown that a dipole PSF is a better fit for GNRs [14]. However, any fit that does not take into account movement must be distorted.

The effect of movement between slices impacts on other work in this study, for which it had been assumed the positional accuracy was $\lesssim 10$ nm. Mitchalet's prediction that only 2 points should be used for extracting the diffusion coefficient from MSD plots was valid for reduced localisation

Version of March 22, 2016– Created March 22, 2016 - 11:05

error $x << 1$ (See section 1.4). The lowered positional accuracy due to movement between slices results for slow diffusive movement in a maximum $x = 0.9$, which according to Mitchalet's formula means $n = 3$ fitting points should be used in MSD plots to optimise the accuracy of extracting the diffusion coefficient, which is only a small change from $n = 2$. However, the tests concerning optimising the extraction of the velocity may also be affected, so this work should be repeated with the revised positional accuracy.

Chapter 4

Conclusion

The most important result was that movement between slices distorts the 3D intensity distribution of a particle in a fluorescence image, resulting in inaccurate fitting, and so lower positional accuracy, particularly for fast diffusing particles. For stationary particles it was found the positional accuracy depended on the separation between the 2D slices in the 3D stack. A smaller separation results in more slices focussed on the particle, so collecting more photons and increasing the accuracy. In typcial experimental conditions the accuracy was found to range from 5.2 ± 0.3nm for stationary GNRs to 31.8 ± 2.5nm for the fastest expected diffusing GNRs.

We verified the prediction of Qian [7] for the relative error in extracting the diffusion coefficient, though found there was a bias to underestimate it. We verified Mitchalet's [8] prediction for the optimal number of fitting points for accurately extracting parameters of motion, however that work should be revisited considering effect of movement between slices on the positional accuracy. We found that fixing the positional accuracy when fitting MSD plots improves the fit, particularly for short trajectories - on average 6.5%.

Finally, we found that Welsh's test can be used to identify transitions in a trajectory, using diffusion coefficient time-series data extracted from MSD plots. The MSD plots are created from windows throughout the trajectory of length N_w. The test compares two samples of size N_s either side of time t in the data, and determines the likeliness they are described by the same distribution (or of the same mode of action). We found that the transitions were most clearly identified by using small windows to calculate the MSD with large samples for Welsh's test - however this work also relies on the positional accuracy, so this too should be revisited considering effect of movement between slices.

Appendix

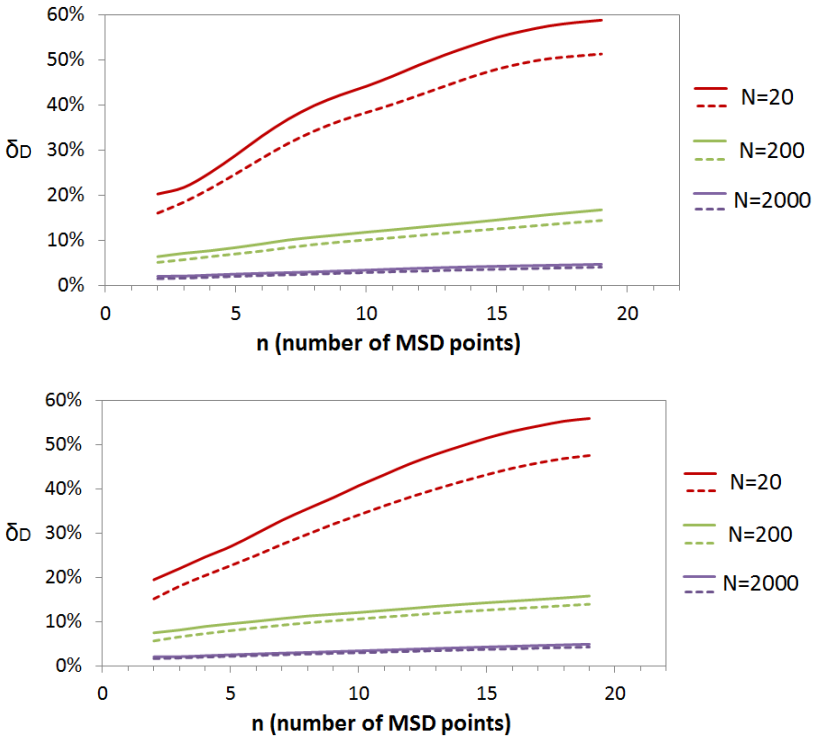

Figure 4.1: Fixing the positional uncertainty σ_p reduces the relative error δ_D in extracting the diffusion coefficient. *The solid lines represent the case where both σ_p and D are fitted, and only $v = 0\,\mathrm{m\,s^{-1}}$ is fixed. The dashed lines show the case where $\sigma_p = 10\,\mathrm{nm}$ is also fitted. 100 purely diffusive trajectories were simulated and analysed with $\sigma_p = 10\,\mathrm{nm}$, $D = 0.01\,\mu\mathrm{m^2\,s^{-1}}$ (top), $D = 0.5\,\mu\mathrm{m^2\,s^{-1}}$ (bottom), over a range of trajectory lengths N. The resulting MSD plots were fit with equation 2.6 using a range of fitting points n. See also figure 2.11.*

(a) $v = 0.01\,\mu\mathrm{m\,s}^{-1}$, $N = 200$

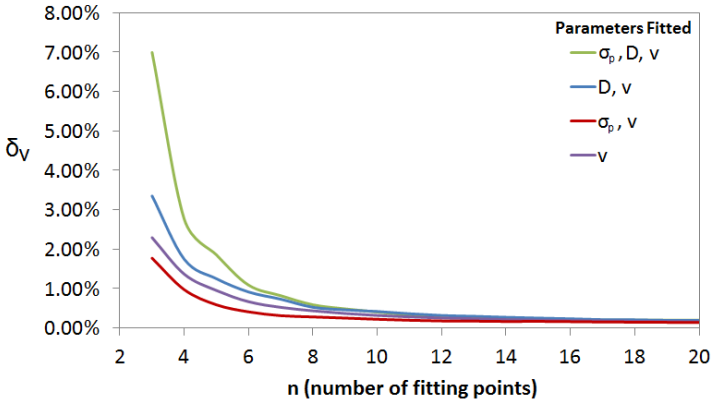

(b) $v = 0.01\,\mu\mathrm{m\,s}^{-1}$, $N = 2000$

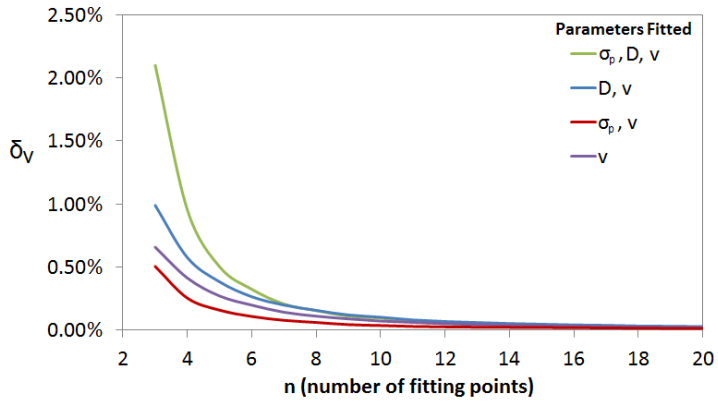

Figure 4.2: Velocities extracted from longer trajectories are more accurate. *The graph shows that increasing the length of a trajectory decreases the relative error as expected. For the same velocity, $v = 0.01\,\mu\mathrm{m\,s}^{-1}$ and positional accuracy $\sigma_p = 10\,\mathrm{nm}$, results from different length trajectories show the same shape curves. For $N = 20$, see figure 2.12.*

References

[1] Laurent Cognet, Cécile Leduc, and Brahim Lounis. Advances in live-cell single-particle tracking and dynamic super-resolution imaging. *Current opinion in chemical biology*, 20:78–85, 2014.

[2] Valeria Levi, QiaoQiao Ruan, and Enrico Gratton. 3-d particle tracking in a two-photon microscope: application to the study of molecular dynamics in cells. *Biophysical journal*, 88(4):2919–2928, 2005.

[3] Bram van den Broek, Brian Ashcroft, Tjerk H Oosterkamp, and John van Noort. Parallel nanometric 3d tracking of intracellular gold nanorods using multifocal two-photon microscopy. *Nano letters*, 13(3):980–986, 2013.

[4] Michael J Rust, Mark Bates, and Xiaowei Zhuang. Sub-diffraction-limit imaging by stochastic optical reconstruction microscopy (storm). *Nature methods*, 3(10):793–796, 2006.

[5] Fabien Pinaud, Samuel Clarke, Assa Sittner, and Maxime Dahan. Probing cellular events, one quantum dot at a time. *Nature methods*, 7(4):275–285, 2010.

[6] Russell E Thompson, Daniel R Larson, and Watt W Webb. Precise nanometer localization analysis for individual fluorescent probes. *Biophysical journal*, 82(5):2775–2783, 2002.

[7] Hong Qian, Michael P Sheetz, and Elliot L Elson. Single particle tracking. analysis of diffusion and flow in two-dimensional systems. *Biophysical journal*, 60(4):910, 1991.

[8] Xavier Michalet. Mean square displacement analysis of single-particle trajectories with localization error: Brownian motion in an isotropic medium. *Physical Review E*, 82(4):041914, 2010.

[9] Winfried Denk, James H Strickler, and Watt W Webb. Two-photon laser scanning fluorescence microscopy. *Science*, 248(4951):73–76, 1990.

[10] Da-Shin Wang, Fu-Yin Hsu, and Chii-Wann Lin. Surface plasmon effects on two photon luminescence of gold nanorods. *Optics express*, 17(14):11350–11359, 2009.

[11] Susie Eustis and Mostafa A El-Sayed. Why gold nanoparticles are more precious than pretty gold: noble metal surface plasmon resonance and its enhancement of the radiative and nonradiative properties of nanocrystals of different shapes. *Chemical society reviews*, 35(3):209–217, 2006.

[12] Haifeng Wang, Terry B Huff, Daniel A Zweifel, Wei He, Philip S Low, Alexander Wei, and Ji-Xin Cheng. In vitro and in vivo two-photon luminescence imaging of single gold nanorods. *Proceedings of the National Academy of Sciences of the United States of America*, 102(44):15752–15756, 2005.

[13] Ernst Abbe. Vii.—on the estimation of aperture in the microscope. *Journal of the Royal Microscopical Society*, 1(3):388–423, 1881.

[14] Eric J Titus and Katherine A Willets. Accuracy of superlocalization imaging using gaussian and dipole emission point-spread functions for modeling gold nanorod luminescence. *ACS nano*, 7(7):6258–6267, 2013.

[15] Albert Einstein. The theory of the brownian movement. *Ann. der Physik*, 17:549, 1905.

[16] Xavier Michalet. Erratum: Mean square displacement analysis of single-particle trajectories with localization error: Brownian motion in an isotropic medium [phys. rev. e 82, 041914 (2010)]. *Physical Review E*, 83(5):059904, 2011.

[17] Bernard L Welch. The generalization of "Student's" problem when several different population variances are involved. *Biometrika*, pages 28–35, 1947.

Version of March 22, 2016– Created March 22, 2016 - 11:05